Impact of Atmosphere Turbulence on Satellite Navigation Signals

Per Høeg, Ramjee Prasad, Kai Borre

Aalborg University
Institute of Electronic Systems
Niels Jernes Vej 14, 9220 Aalborg, Denmark
Phone: +45 9635 9828, Fax: +45 9815 1583, e-mail: hoeg@kom.aau.dk

Abstract. Atmosphere turbulence for low elevation angle reception is a noise source that is not well defined in existing systems using satellite navigation signals. For high precision aviation purposes atmosphere turbulence needs to be assessed to meet the future stringent requirements.

High precision receivers using open-loop mode data sampling at high sampling rate enables investigations of the characteristics of the noise and the multi-path signal errors through the determination of the refractive index structure constant C_n^2. The main modulation of GPS signals in low-elevation measurements is attenuation and frequency shift due to ray bending. Whereas the presence of turbulence results in a spectral broadening of the signal. Analysis of the trends of the spectral mean slope for different frequency domains will be discussed in relation to the characteristics of atmosphere turbulence. Additionally we present results from phase-lock receivers loosing lock during strong perturbations.

1 Introduction

High altitude field tests have established experimental knowledge on the influence of atmosphere turbulence on receiver performance in tropical regions [1]. Moist air turbulence measurements from Haleakala, Hawaii, are studied and presented here for spectral signal structure characteristics.

The performed spectral properties of the received signals by a high precision GPS instrument in both phase-locked mode (PL) and open-loop mode (OL) are compared to theoretical results. PL or closed loop tracking is the standard technique used by most GPS receivers. It reduces the needed bandwidth of the measurements by having the carrier phase locked to the received signal. Open loop tracking (OL) or raw mode sampling requires the full measurements relatively to an on-board Doppler model. The method requires more advanced receivers with high sampling rates. The advantage is the full information on phase and amplitude, which reduces relative errors in the signal-to-noise ratio.

The OL mode of the applied GPS instrument provides sampling rates up to 1000 Hz, which enables investigation of spectral signatures that are normally not seen in GPS data [2, 3]. The use of directive antennas pointed towards the horizon give signal recordings down to the lowest layers of the atmosphere.

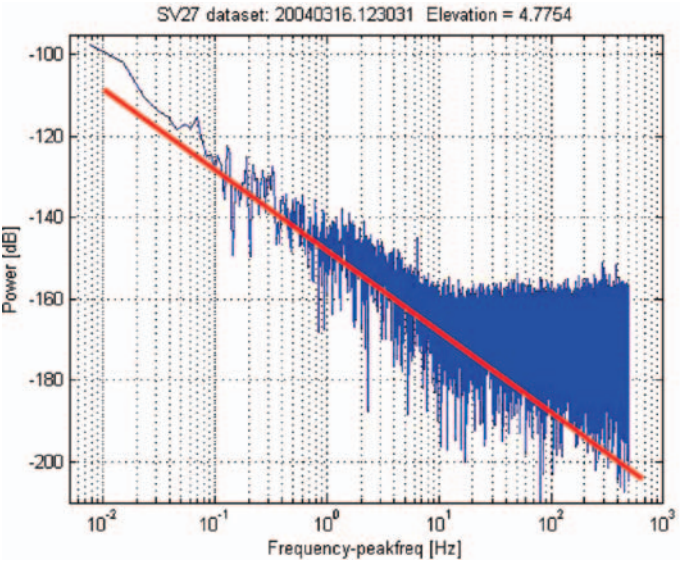

Fig. 1. Spectral characteristics for turbulence conditions.

Figure 1 shows a spectrum for a low-elevation measurement in raw mode sampling (OL) when turbulence is present in the direction towards the transmitting GPS satellite.

The high-frequency part of the signal, for frequencies larger than 100 Hz, is dominated by thermal noise. While the lower frequency part is dominated by clock-noise, which for the receiver rubidium clock falls off as the inverse of the frequency squared. So in order to study atmospheric low-elevation turbulence by spectral analysis, we investigated spectral fluctuations above the noise characteristics of the clock caused by the turbulent atmosphere.

The experiments are from the top of Haleakala at an altitude of more than 2500 meters (Fig. 2). The analysis focuses on observations from the south-west, since most measurements in this geometry of ascending and descending GPS trajectories are close to a vertical plane surface. This geometry leads to faster scanning of the troposphere, which makes it possible to compare results from different altitude regions of the troposphere. Additionally, this sector also turned out to have the lowest multipaths reflections from the nearby islands and objects on the islands.

2 Instrumental Setup

The instrument setup consists of separate L1 and L2 antennas placed right next to each other and oriented with the main gain lobe toward the horizon. The signals are fed into a prototype version of a satellite high precision GPS receiver (Fig. 3), where the instrument software is modified for ground-based signal Doppler conditions. An ultra-stable rubidium frequency reference is used to control the receiver clock for

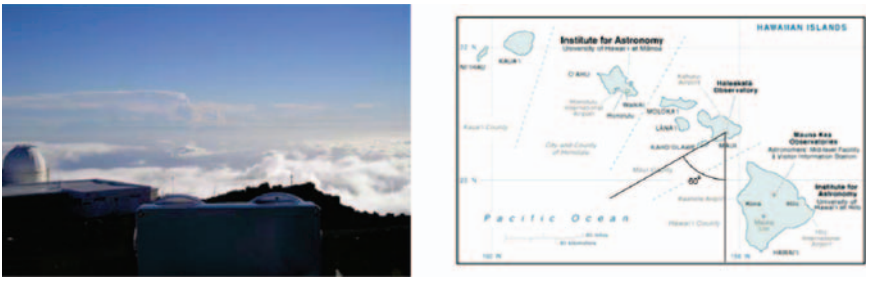

Fig. 2. Left panel is a picture of the field of view for the observations, which for most of the time in the horizontal direction is above the clouds. The adjacent panel gives the directional cone for the observation presented here.

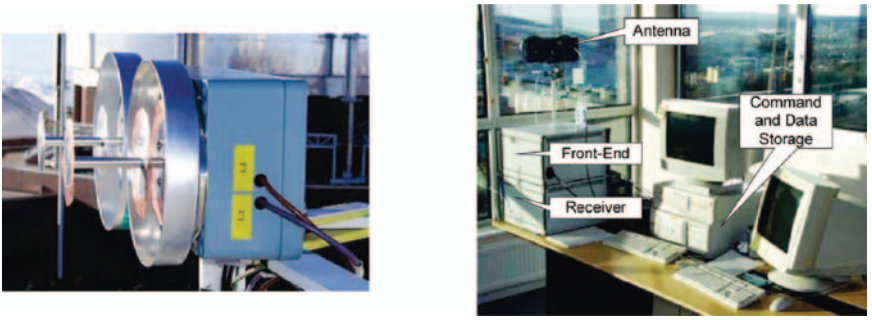

Fig. 3. Left panel shows the applied antenna type. While the picture on the right shows the prototype high precision GPS receiver used for the observations.

precise timing of the measurements. Signals are tracked in both PL and OL mode at the same time in separate receiver channels.

3 Experimental Results

During multi-path conditions, traditional PL tracking receivers may loose signal lock and hence fail to track the signal. During multi-path situations, where rapid phase and amplitude variations occur, signal conditions cause the PL tracking to fail.

The complex signal strength at the antenna is given as,

$$V_{Ant}(t(n,m)) = \sqrt{G_k^{-1}(ch)} \cdot (I(n,m) + jQ(n,m)) \cdot e^{j\varphi(t)}$$

where, t represents the time (at data packet number n and sample number m), $G_k\,(ch)$ the receiver gain for channel ch at wave number k. I and Q are the quadrature amplitudes, while φ is the phase. For coherent signals (Fig. 4) the I and Q terms give a unique solution. While for non-coherent signals, as is the case for the data presented in this paper, the spectral spread gives a multitude of solutions. PL-based receivers loose lock under these conditions since no unique solution is possible to identify.

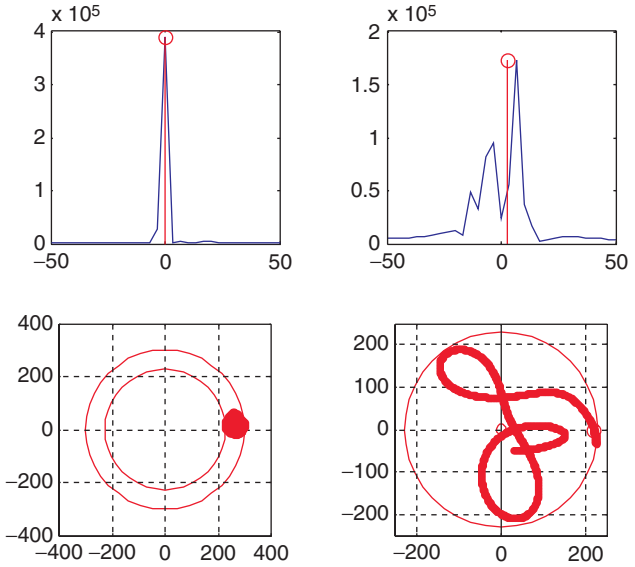

Fig. 4. Power spectra (upper panels) and their respective *I* and *Q* measurements (lower panels) for coherent (left graphs) and non-coherent atmosphere conditions (right graphs). The observations to the right represent the general situation when atmosphere turbulence is present.

The OL data sampling rate of 1000 Hz enables detection and investigation of the characteristics of the noise and the multi-path signal error sources through the determination of the refractive index structure constant C_n^2 of the atmosphere turbulence [4, 5]. The main atmospheric modulation of GPS signals in low-elevation measurements is attenuation and frequency shift due to ray bending, whereas the presence of turbulence is causing a spectral broadening of the signal. Displaying the power spectrum as function of frequency difference from the main signal peak reveals the characteristic domains of the spectrum. Up to 10 Hz, the spectrum is approximately sloping as the inverse of the frequency squared (Fig. 1). While for higher frequencies, in the range 10–500 Hz, the spectrum flattens. The latter part of the spectrum originates from thermal noise, while the first sloping part is characteristic for the rubidium frequency reference used in both the GPS transmitter and the receiver [6]. Analysis of the trend of the mean slope in the spectra for different frequency domains showed an increased slope as function of the elevation of the received signal above the horizon, indicating turbulence and eddies in the beam direction [1].

Here we shall focus on the observations, where meteorological conditions have an important impact on the generation of atmosphere turbulence. Most conditions are driven by either dynamical phenomena (as large vertical winds, horizontal wind shear, mountain lee waves or gravity waves) or ther-modynamically unstable air mass conditions (strong high/low pressure systems, some types of clouds, and lightning). The five time-series chosen here depict the generation of enhanced turbulence and larger inner scale lengths for the dissipative processes of the scintillations during

such conditions. The horizontal wavelengths are estimated to range from 0.5 m to 10 km, with vertical extents of 100–2000 m.

The *orange* dataset in Fig. 5 are from a meteorological situation, where the magnitude of the wind is decreasing with low vertical wind components. The gradients in the pressure surfaces are at the same time increasing. During the *red* time series the winds are very variable with high vertical wind speeds and large gradients in the temperature and the pressure. The *blue* and the *red* datasets are during similar atmosphere conditions. The difference is that in the *blue* set lower vertical winds speeds are observed.

The spectral changes as function of elevation angle show a broadening once the turbulent layers are in the field-of-view of the direct signal. The right panel in Fig. 6 shows the enhanced variances from the turbulent region. The turbulent layers show a lot of vertical fine structure with vertical extents smaller than 100 m.

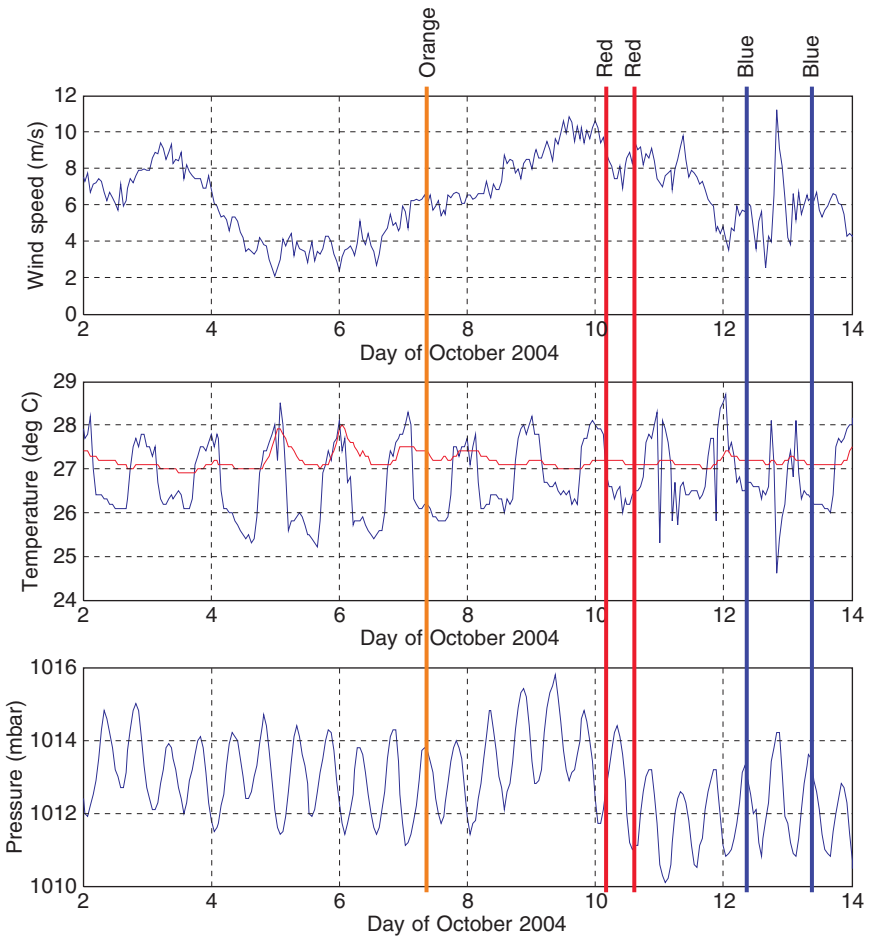

Fig. 5. Wind, temperature and pressure conditions during situations of spectral turbulence for the monitored region of troposphere. The orange, red and blue datasets are marked since they describe meteorological conditions leading to weak and strong turbulence.

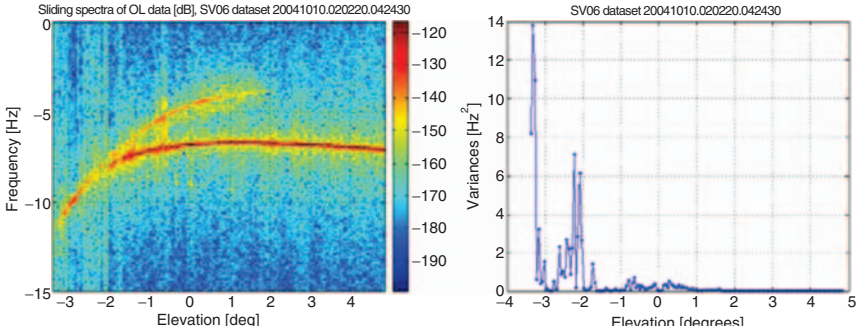

Fig. 6. Stack plot of power spectra in the left panel. Both the direct and the ocean-reflected signal are present. The right panel gives average variances for the turbulent troposphere in the first time series of the *red* datasets.

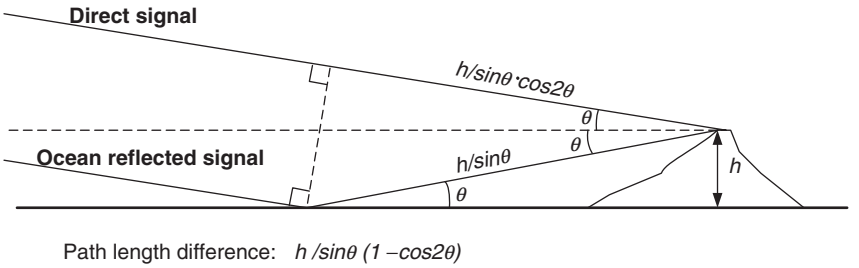

Fig. 7. Schematic presentation of the received signals for low elevation angle measurements.

Apart from the direct signal, having the highest power, the spectra also show the ocean-reflected signal, which can be seen in Fig. 6 for elevation angles lower than 3 degrees. Fig. 7 gives a schematic presentation of the geometry leading to the two main spectral signals.

The prominent characteristic scales of the turbulence region are confined between the outer scale L_0 and the inner scale l_i of the turbulence [4, 5]. For scale lengths larger than the outer scale, eddies introduce kinetic energy into the turbulence region. While eddies smaller than the inner scale remove kinetic energy through dissipative processes. Applying these assumptions leads to the definition of the amplitude variance and the turbulence structure constant [7, 8].

$$\sigma_\chi^2 = \int_0^L C_n^2(x)\left[\frac{\chi(L-\chi)}{L}\right]^{5/6} dx$$

$$C_n^2 = C_{n,0}^2\, e^{-\left[\frac{h}{H} + \frac{(x - L1)^2}{2(R_E + h)H}\right]}$$

$C_{n,0}^2$ is the turbulence structure constant for the given region. L is a characteristic scale length, R_E is the radius of the Earth, h the altitude of the region in the

atmosphere, and H the atmospheric scale height for the turbulence region. Assuming that the turbulent layers has a scale size relation as,

$$a^2 = b(R + z_0)$$

leads to the definition of five different regions of turbulence for the presented observations [8]. Here, a is the horizontal extend of the turbulent layer, b the scale height of the structure constant, and z_0 the tangent altitude of the line-of-sight. The next chapter contains an estimation of the regions that specifically defines the observed turbulence.

Figures 8 and 9 show observational time series from the *orange* and the *blue* meteorological conditions. The vertical extent of the turbulence region is quite different from the situations in the *red* datasets. For the *orange* situation (Fig. 8) the weak turbulent layers cover altitudes from above the boundary layer up to altitudes of 5 km with a lot of vertical fine structure. The situation in the Fig. 9 (the *blue* data sets) is mostly related to the troposphere processes in the last two kilometers above the surface of the ocean, leading to less fine vertical structures.

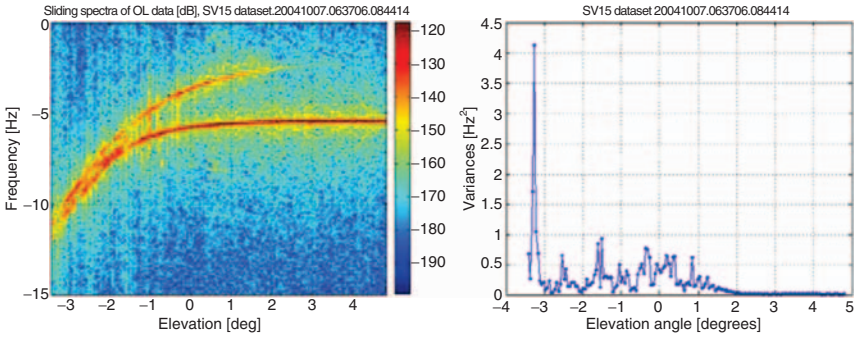

Fig. 8. Power spectra stack plot (left panel) and variances for the turbulent troposphere in the *orange* dataset.

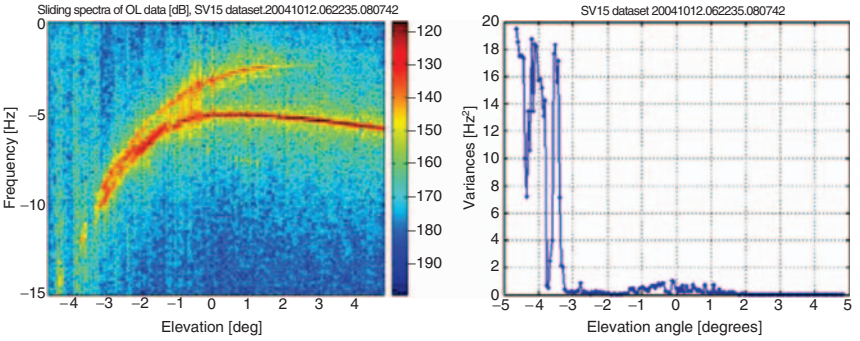

Fig. 9. Power spectra stack plot (left panel) and variances for the turbulent troposphere in the *blue* datasets.

4 Discussions

All the spectral information of turbulence for the presented datasets shows a strong resemblance to the region 2 and 3 variances, defined in [8]. Region 2 and 3 turbulence variances becomes respectively,

$$\sigma_\chi^2 = C_2 k^2 L_0^{5/3} a C_n^2$$
$$\sigma_\chi^2 = C_3 k^3 L_0^{8/3} (ba/L_1) C_n^2$$

for situations when the product of the wavelength and the characteristic turbulence scale height is much larger than the outer scale length squared and much smaller than the product of the scale height of the structure constant and the outer scale length [8, 7, 5]. The conclusions from our measurements follow nicely other similar observational results [9]. They found for 9.6 and 34.5 GHz frequency measurements a power law relation in the power spectra with a mean slope of –8/3, which is similar to the region 3 variances. Our analysis of the statistical estimates of the mean slopes (for the frequency interval 0.1–10 Hz) for our observations gives slopes ranging from –2.8 to –1.5.

5 Conclusions

We have shown that high precision open-loop GPS receivers are capable of determining the troposphere turbulence in tropical regions. The OL observations revealed characteristics of the vertical layering of turbulence. For the strongest cases the vertical fine structure becomes less than 100 m. During such cases it was also identified that standard PL receivers loose signal lock. The dominant cause for the presence of troposphere turbulence is a combination of larger vertical wind components combined with thermodynamically unstable air driven by temperature and pressure gradients. This is also reflected in the spectral variances for the layers, which directly link to the turbulence structure function constant. The statistical analyses of all the measurements lead to region 2 and 3 turbulence with spectral slopes varying from –2.8 to –1.5.

References

[1] L. Olsen, A. Carlström, and P. Høeg, "Ground Based Radio Occultation Measurements Using the GRAS Receiver", ION 17th Sat. Div. Techn. Meeting, Proceedings, ION, pp. 2370–2377, 2004.

[2] P. Høeg, M.S. Lohmann, L. Olsen, H.H. Benzon, and A.S. Nielsen, "Simulations of Scintillation Impacts on the ACE+ Water Vapour Retrieval Using Satellite-to-Satellite Measurements", ESA Atmos. Remote Sensing Symposium, Proceedings, ESA, pp. 148–161, 2003.

[3] P. Høeg, and F. Cuccoli, Measuring Atmosphere Turbulence, Humidity, and Atmospheric Water Content (MATH-AWC). ESA Science Report, ESA, EOP-SM–1297, 2005.

[4] V. I. Tatarskii, The Effects of the Turbulent Atmosphere on Wave Propagation. U.S. Dept. of Commerce, Springfield, USA, 1971.

[5] A. D. Wheelon, Electromagnetic Scintillations. I. Geometrical Optics. Cambridge Univ. Press, Cambridge, 2001.
[6] A. S. Nielsen, M. S. Lohmann, P. Høeg, H.-H. Benzon, A. S. Jensen, T. Kuhn, C. Melsheimer, S. A. Buehler, P. Eriksson, L. Gradinarsky, C. Jiménez, G. Elgered, Characterization of ACE+ LEO-LEO Radio Occultation Measurements. ESA Science Report, ESA, 16743–2, 2003.
[7] A. Ishimaru, Wave Propagation and Scattering in Random Media, Vol. 2. Academic Press, New York, USA, 1978.
[8] R. Woo and A. Ishimaru, "Effects of Turbulence in a Planetary Atmosphere on Radio Occultation", IEEE Transactions on Antennas and Propagation, AP-22, pp. 566–573, 1974.
[9] H. B. Janes, M. C. Thompson and D. Smith, "Tropospheric Noise in Microwave Range-Difference Measurements", IEEE Transactions on Antennas and Propagation, AP-21, No. 2, pp.566–573, 1973.